nature chemistry

ARTICLES

PUBLISHED ONLINE: 7 NOVEMBER 2016 | DOI: 10.1038/NCHEM.2641

Self-assembly of nanoparticles into biomimetic capsid-like nanoshells

Ming Yang[1,2,3], Henry Chan[4], Gongpu Zhao[5], Joong Hwan Bahng[2,6], Peijun Zhang[5,7]*, Petr Král[4,8,9]* and Nicholas A. Kotov[1,2,6,10,11]*

Nanoscale compartments are one of the foundational elements of living systems. Capsids, carboxysomes, exosomes, vacuoles and other nanoshells easily self-assemble from biomolecules such as lipids or proteins, but not from inorganic nanomaterials because of difficulties with the replication of spherical tiling. Here we show that stabilizer-free polydispersed inorganic nanoparticles (NPs) can spontaneously organize into porous nanoshells. The association of water-soluble CdS NPs into self-limited spherical capsules is the result of scale-modified electrostatic, dispersion and other colloidal forces. They cannot be accurately described by the Derjaguin–Landau–Vervey–Overbeek theory, whereas molecular-dynamics simulations with combined atomistic and coarse-grained description of NPs reveal the emergence of nanoshells and some of their stabilization mechanisms. Morphology of the simulated assemblies formed under different conditions matched nearly perfectly the transmission electron microscopy tomography data. This study bridges the gap between biological and inorganic self-assembling nanosystems and conceptualizes a new pathway to spontaneous compartmentalization for a wide range of inorganic NPs including those existing on prebiotic Earth.

A simple yet versatile geometry of nanoshells is at the foundation of their many unique physical, chemical and biological properties. Nanoshells with subnanometre pores are frequently used in nature to sustain gradients of pressure, pH and ion concentration. They also allow compartmentalization of chemical components in liquids and so provide reaction control, selective transport, protection and reconfigurable sites for homogeneous catalysis. Biomolecular nanoshells are typically formed by the self-assembly of tens to a few thousands of organic structural units that are either highly anisotropic, for example, phospholipids that form a membrane in vacuoles, transport vesicles and so on, or bound together by highly specific lock-and-key interactions found, for instance, between structural proteins of viral capsids[1], cellular vesicles[2], exosomes[3], carboxysomes[4] and bacterial bubble compartments[5].

Inorganic nanoshells are being actively studied for their unique optical[6], mechanical[7] and catalytic[8] characteristics that often originate in shell-confined quantum mechanical effects. Templating composite films on spherical particles affords artificial nanoshells with diameters that range from several hundreds of nanometres to several micrometres[9]. The Kirkendall effect[10], non-equivalent stoichiometry reactions[11] and Oswald ripening[12] lead to the formation of 10–200 nm nanoshells by chemical transformation of nanoparticles (NPs) using mismatches between ion exchange and diffusion rates for different ions.

The chemical methods laid in the foundation of inorganic nanoshell formation are conceptually different from those utilized by nature based on the self-assembly of bioorganic units with specific molecular geometries. Besides the technological significance of inorganic nanoshells, their spontaneous formation from simple nanoscale units can shed light on the genesis of compartmentalized structures in nature and, perhaps, life itself. However, this may appear fundamentally prohibited without atomically precise spherical tiling of the structural units or highly anisotropic molecule-building organic blocks, for instance lipids. Compared with proteins, lipids or polymers[13], inorganic nanoscale building blocks will impart new properties and functions to nanoshells. For instance, controllable porosity, stability and reconfigurable geometry of the biomimetic nanoshells would be essential for the homogeneous catalysis of 'difficult' reactions and structurally responsive systems. The self-assembly of inorganic shells from NPs will also be insightful for self-healing and biomineralization processes that lead to nanoshell formation in living organisms[14].

The studies carried out over the past decade indicate that inorganic NPs display a distinct ability to self-organize into terminal structures (supraparticles[15], nanostars and so on) and extended structures (chains[16], sheets[17], superlattices[18,19] and others), but they were not observed to form shells or other open structures or spontaneously formed compartments. Here we demonstrate that simple CdS NPs do produce porous nanoshells and elaborate the mechanism of their formation. Their assembly from simple structural units without pronounced hydrophobic/hydrophilic anisotropy, lock-and-key interaction or molecular tiling between the constituents is attributed to a specific interplay of repulsive and attractive forces between NPs, ions and solvent that favours exclusion of NPs from the centre of these assemblies. Despite the generality of approaches and forces involved, the nanoshell formation cannot be rationalized fully based on traditional colloidal theories. However, it can be understood using molecular dynamics (MD) simulations with an atomistic description of NPs, surface ligands, counterions and solvent molecules. Progressive coarse graining of

[1]Department of Chemical Engineering, University of Michigan, Ann Arbor, Michigan 48109, USA. [2]Biointerfaces Institute, University of Michigan, Ann Arbor, Michigan 48109, USA. [3]Key Laboratory of Microsystems and Micronanostructures Manufacturing, Harbin Institute of Technology, Harbin 150080, China. [4]Department of Chemistry, University of Illinois in Chicago, Chicago, Illinois 60607, USA. [5]Department of Structural Biology, School of Medicine, University of Pittsburgh, Pittsburgh, Pennsylvania 15260, USA. [6]Department of Biomedical Engineering, University of Michigan, Ann Arbor, Michigan 48109, USA. [7]Department of Mechanical Engineering and Materials Science, Swanson School of Engineering, University of Pittsburgh, Pittsburgh, Pennsylvania 15260, USA. [8]Department of Physics, University of Illinois in Chicago, Chicago, Illinois 60607, USA. [9]Department of Biopharmaceutical Sciences, University of Illinois in Chicago, Chicago, Illinois 60612, USA. [10]Department of Material Sciences and Engineering, University of Michigan, Ann Arbor, Michigan 48109, USA. [11]Michigan Center for Integrative Research in Critical Care, Ann Arbor, Michigan 48109, USA. *e-mail: pez7@pitt.edu; pkral@uic.edu; kotov@umich.edu

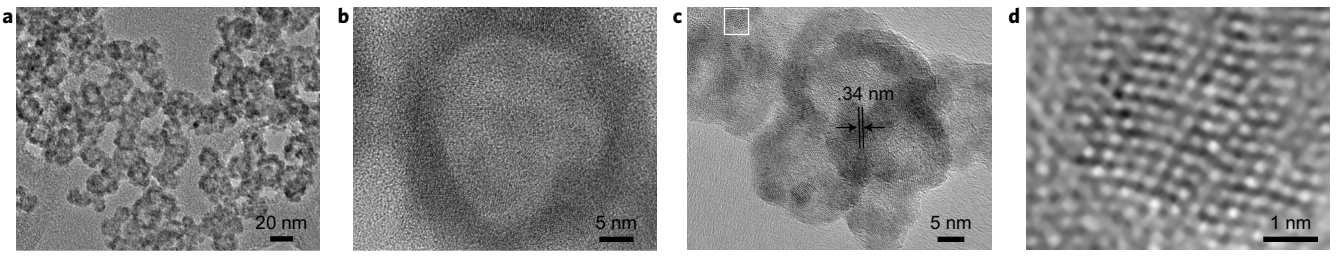

Figure 1 | Nanoshells spontaneously form from 'naked' polydispersed inorganic NPs. a, A TEM image of CdS nanoshells (22 ± 4 nm) obtained at pH 9.5. These nanoshells share similarities with capsids, but consist of small inorganic NPs (3–5 nm) without apparent structural anisotropy, precise molecular tiling and specific lock-and-key interaction. **b**, A high-resolution TEM image of a CdS nanoshell shows the packing of the constituent NPs on the surface; the thickness of the nanoshell corresponds to a monolayer of NPs. **c**, A high-resolution TEM image of several nanoshells showing crystal lattices of (111) planes of cubic CdS. **d**, The enlarged high-resolution image of the area in the white rectangle in **c** that can be associated with the constituent NP tetrahedron.

NP interactions from fully atomistic MD with an *ab initio* calculation of the atomic charges to a partially atomistic description with a Hamaker approximation of core–core dispersion forces allows one to balance the accuracy of the structural description with an effective experimental time window to reveal the conditions necessary for nanoshells to form.

Results

Constituent NPs. CdS NPs were used in this study as a model structural unit known to be capable of self-organization; these NPs are representative of other semiconductor nanocolloids in respect to the size, shapes and physical/chemical properties. Nanoshells with diameters of 20–50 nm (Fig. 1a,b) formed during the combined process of synthesis and assembly, reminiscent of the protein-assisted self-assembly processes[19]. The pH of the reaction media and final nanoshell dispersion was controlled by 0.01 M NaOH solution and in most experimental series was 9.5. Besides thioacetamide serving as the source of sulfur and decomposing in the reaction, no extraneous organic molecules known as stabilizers or surface ligands, that typically coat NP surfaces were used. This structural characteristic is attractive not only for the simplicity of the synthetic protocol, but also for modelling; low concentration and affinity of decomposition products of thioacetamide to CdS makes possible to consider these NP essentially 'naked'.

Nanoshell formation and structure. Individual NPs, as assembly units of the nanoshells, can be identified in transmission electron microscopy (TEM) images by the presence of crystalline interfaces visible at high magnification. Their lattice spacing of 0.34 nm corresponds to the (111) crystal planes (Fig. 1c,d) and is typical for cubic CdS. The oriented attachment observed for other NPs[16,20,21] did not contribute to the spherical tiling of CdS NPs because it occurs at a much slower rate than for CdTe[16] and PbS[22] and for symmetry considerations. The wall thickness of these nanoshells was 3–5 nm and was identical to the dimensions of the NP 'building blocks' (Supplementary Fig. 3a).

Room-temperature and cryo-TEM tomography of rapidly frozen samples captured the assemblies in their native hydrated state (Fig. 2a–d, Supplementary Movie 1) and confirmed the formation of nanoshells. The three-dimensional (3D) arrangement of the constituent units can be described accurately by this technique, which makes possible a direct juxtaposition of the microscopy data with computer modelling[23]. The multiplicity of NPs in the nanoshells and the long time required for dynamic NP systems to reconfigure make this system particularly difficult to simulate compared with those of other studies (Supplementary Note 1). The wall thickness of ~4–5 nm and the diameter of ~10–15 nm for the nanoshells observed from cryo-TEM tomography were consistent with the data in Fig. 1. That the shells were composed of NPs without any special geometrical fit to each other was evident in these images and could be further highlighted by the 3D surface rendering of the nanoshell with identified CdS domains (Fig. 2e, the slice view of the raw reconstruction can be found in Supplementary Figs 4,5). TEM imaging demonstrates that a nanoshell with a diameter of 20 nm accommodated about 90 NPs. The presence of nanoscale pores with a diameter of ~2 nm between the constituent NPs can be observed (Fig. 2c,d).

TEM images taken in the course of the nanoshell synthesis and assembly revealed intermediate geometrical shapes that led eventually to the formation of nanoshells. After five minutes, NPs form small arc-shaped agglomerates (Fig. 3a,b). After ten minutes, they transform into incomplete crescent-like formations (Fig. 3c,d). The closing of the shells occurs in the subsequent 20 minutes of the assembly (Fig. 3e,f). Again, no preferred contact surfaces, geometrically matching shapes or substantially larger agglomerates—chains[16], sheets[17], ribbons[24] and so on observed in similar systems—could be identified at any stage of the process. Nanoshells and some individual NPs were exclusive products of this process, with nanoshells representing over 90% of the NPs.

Assembly conditions and nanoshell structure. The self-organization of NPs into nanoshells was found to be pH dependent. At pH 8.2 and 7.2, nanoshells with diameters of 16 ± 2 nm, which contained ~58 NPs (Supplementary Fig. 6), and 11 ± 2 nm, which contained ~22 NPs (Supplementary Fig. 7), were observed. In each case the number of NPs and the size of the nanoshells were smaller than those formed at pH 9.5 with diameters of 22 ± 4 nm (Fig. 1). Statistical analysis showed that the sizes of the constituent NPs captured at the earlier stage of assembly were similar under different pH conditions: 4 ± 0.8 nm for pH 9.5, 4 ± 0.8 nm for pH 8.2 and 4 ± 0.7 nm for pH 7.2 (Supplementary Fig. 3). Solid supraparticles that contained ~20 structural units and could be described as imploded shells appeared when the assembly process was carried out at pH 5 (Supplementary Fig. 8a–c). At pH 4.3, predominantly single NPs were present (Supplementary Fig. 8d–f).

An increase in pH coincides with an increase of the zeta potential, ζ, of the nanoshells. At pH 7.2, we observed nanoshells with $\zeta = -11 \pm 1$ mV. This electrokinetic potential can be related to a total surface charge of $Q_{CdS} = -7.2 \times 10^{-19}$ C, equivalent to ~4–5 electrons per nanoshell (Supplementary Methods; the model used here is based on ion classical colloidal theories for solid spheres; although it provides some assessment of particle charge, its limitations should also be considered.) As ~22 CdS NPs form the nanoshell, the average charge on the individual NPs approximates to $q = -0.2e$. Similarly, at pH 8.2 and pH 9.5, nanoshells displayed $\zeta = -30 \pm 2$ mV and -50 ± 2 mV, respectively, which corresponds to a total surface charge of $Q_{CdS} = -3.7 \times 10^{-18}$ C or -8.9×10^{-18} C, equivalent to, respectively, ~23 or 55 electrons per nanoshell (Supplementary Methods) or an average charge of $q \approx -0.4e$ or $-0.6e$ per NP (about half of the NPs are single charged). As expected, the increase

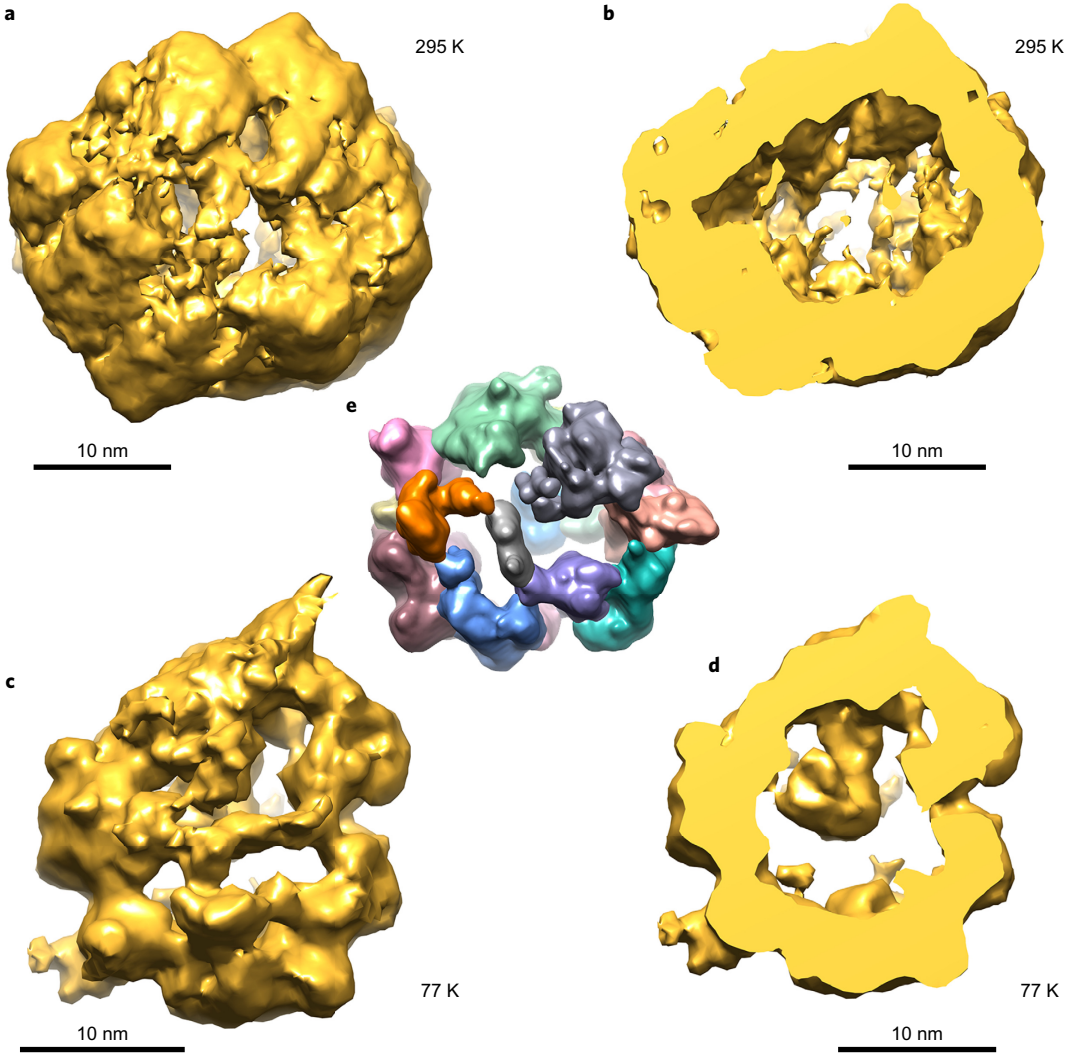

Figure 2 | 3D structure of nanoshells from CdS NPs obtained by TEM tomography. a–d, Surface (**a**,**c**) and cross-section (**b**,**d**) of the nanoshell at room temperature (**a**,**b**) and at cryo-conditions (**c**,**d**), capturing the structural information of the assemblies in their native environment and showing the porous nature of the nanoshells. **e**, 3D surface rendering of the nanoshell with differently coloured NP domains without any special geometric fit. 3D reconstruction of the nanoshells is also given in the Supplementary Movie 3.

of average NP charge leads to an increase of nanoshell size, and electrostatic repulsion between the 'building blocks', enhanced by electro-osmosis, causes the transition of the assembly pattern from cavity-less supraparticles observed before[15,25] to nanoshells.

The essential role of the electrostatic interactions in the emergence of the nanoshell geometry of the assemblies can also be inferred from the effect of ionic strength on the screening of these interactions. We tested such an effect at a condition of pH 9.5, which produced the largest cavities. When the ionic strength was increased from 0.8 to 5.8 mM, instead of nanoshells we observed small 11 ± 2 nm NP clusters (Supplementary Fig. 9a–c). They are still porous, similar to nanoshells (Supplementary Fig. 9b). A further increase of ionic strength to 10.8 mM turned most of the NPs into more-compact structures with even smaller diameters (7 ± 2 nm) (Supplementary Fig. 9d–f); electrostatic repulsion screened by an increased ionic strength is not strong enough for the stabilization of central cavities, which results in denser assemblies and in agreement with the pH influence on the formation of nanoshells and previous observations of supraparticles[15,25].

Discussion

Modelling of the nanoshells at several levels of approximation help us to understand the mechanisms responsible for their formation. The pair-wise interaction energy of NPs is determined by van der Waals (vdW) and electrostatic interactions, with contributions from hydrogen bonding, entropic forces and dipolar interactions[17]. Uniformity of the nanoshell diameter and wall thickness is indicative of the self-limiting growth mode and thermodynamic control typical for terminal self-assembled structures previously observed for cavity-less supraparticles[15,25]. The absence minimization of the surface layer decreases inter-NP gaps and can strengthen both repulsion and attraction simultaneously. The former favours open porous structures, whereas the latter enables nanoshell assembly without the spherical tiling.

Although some aspects of the supraparticle-to-nanoshell transition can be heuristically explained with classical electrostatics using Gauss's Law and formulae for spherical capacitors, these models are not suitable for self-assembled NP structures in liquid matter with electrostatic screening. To describe the NP–NP forces in water, one may use the Derjaguin–Landau–Vervey–Overbeek (DLVO) theory. DLVO approximations traditional for colloids, thermodynamically (meta) stable nanoshells will form when the vectorial sum of the repulsive and attractive forces associated with each spherical NP in the nanoshell (Supplementary Fig. 2a,b) is zero. As a result of the spherical symmetry of the nanoshells, one

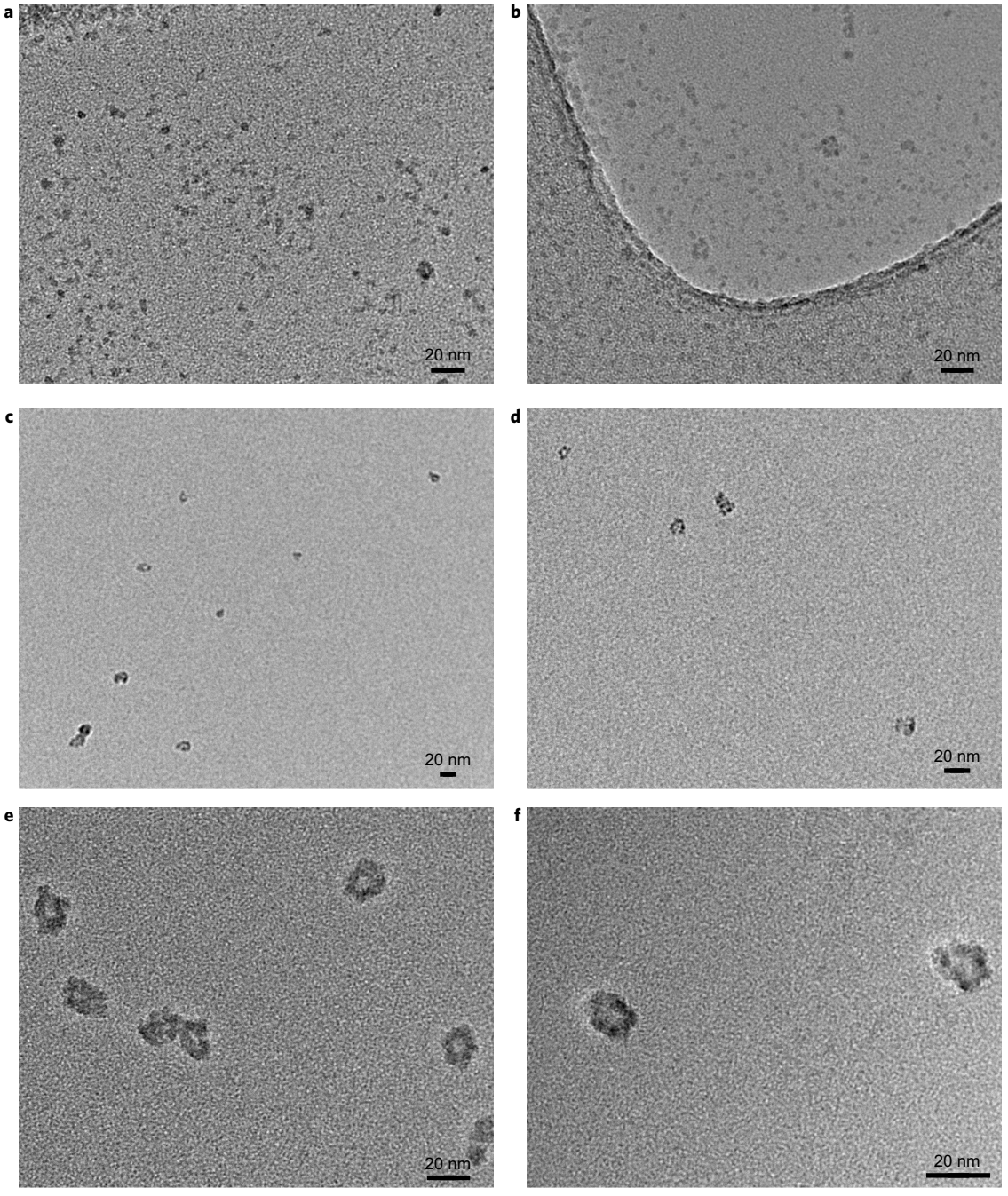

Figure 3 | Temporal progression and intermediate stages of nanoshell assembly that demonstrate the gradual transition from individual NPs to nanoshells. Representative TEM images of CdS nanoshells obtained after the assembly at pH 9.5. **a**,**b**, The presence of individual NPs with the emergence of embryonic forms of nanoshells at 5 min. **c**,**d**, Arc-shaped assemblies as an intermediate precursor for nanoshells appear at 10 min. **e**,**f**, After 20 min complete shells are formed.

can calculate the balance of forces, taking, for instance, a NP located at the selected pole. As one could expect, N, the number of NPs in a nanoshell, is dependent on q, but the overall dependence is opposite to that observed experimentally (Supplementary Fig. 2c). Such a model also predicts that the increase of ionic strength, I, should lead to larger nanoshells, which is again inconsistent with our observations (Supplementary Fig. 2d). Such predictions may seem counterintuitive in the light of shorter distances between NPs. However, the result originates in large part from the fact that the medium is described in DLVO as a continuum dielectric and so it is needed to account for the variable dielectric constant around the NPs[26]. Also, smaller shells include smaller numbers of NPs and thus have lower integral pairwise Coulombic repulsion within the DLVO theory. Modification of the repulsive or attractive components of DLVO that make, for instance, an NP carry special patches or involve additional forces can potentially 'fix' the incorrectly predicted trend. Although for some NPs these assumptions could be helpful, we have no evidence of their validity for the NPs used here. Moreover, the DLVO model typically restricts the building blocks to spheres and uses highly simplified interactions that are difficult to justify for NPs[27].

The variety and complexity of NP–NP interactions in the experimentally observed nanoshells can be accounted for by atomistic MD simulations. Given the ever-increasing computational power and improvements in 3D resolution of the nanoscale structures enabled by TEM (Fig. 2), the combination of these methods represents

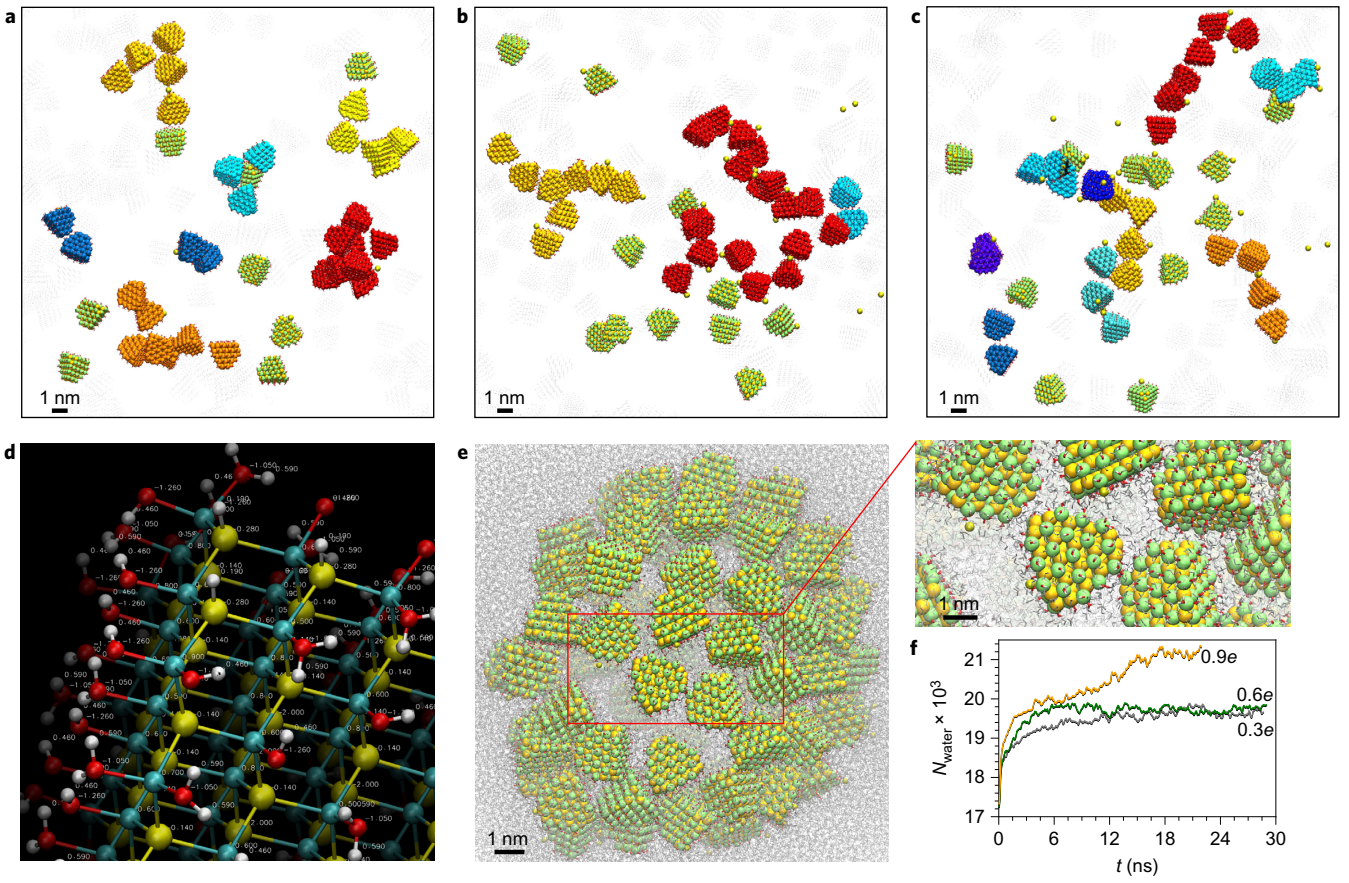

Figure 4 | Model 1 MD simulation of NP self-organization with high atomic precision but short effective assembly times. a–c, Snapshots taken after ~65 ns simulations of assemblies from NPs that carry $q = 0.3e$ (**a**), $0.9e$ (**b**) and $1.34e$ (**c**). Yellow-green units represent individual NPs. Other colours denote assembled NP particles with different degrees of connectivity. Sodium counterions are shown as yellow spheres. Note the extended assemblies from multiple connected particles (red, orange and yellow) that mirror the arc-shaped structures in Fig. 3c,d. **d**, Atomic charges on the NP surfaces and in the cores were calculated with *ab initio* methods using small atomic clusters. **e**, Snapshot after ~22 ns equilibration for pre-assembled NPs that carry $q = 0.9e$. Inset shows an enlarged view of the highlighted region; note the atomistic description of both the surface and media. **f**, Plots for the number of water molecules inside the nanoshells with $q = 0.3e$, $0.6e$ and $0.9e$. Stabilization of the cavity size for $q = 0.3e$ and $0.6e$ is indicative of stabilization of the shell in a (local) thermodynamic minimum.

a powerful toolbox for the understanding of the fast atom-scale reorganization of single NPs (Supplementary Note 1). However, as we can see from the data below, difficult fundamental problems associated with the utilization of these tools for the self-assembly of multiple NPs remain. In this study, we demonstrate one of the pathways that computational work on large NP assemblies can take.

Based on previous studies by Vossmeyer *et al.*[28], the CdS NPs were modelled as tetrahedrons built from atoms of Cd and S in an atomically accurate crystal lattice. As NPs that form the nanoshells in Figs 1–3 are not made with any special surface ligands from extraneous organic component(s) and the NP stabilization effect from decomposition products of thioacetamide can be neglected due to low molecular weight and absence of anchor thiol group, the surface of the NP is modelled as chemical groups typical for aqueous media, for example, H–, OH– and H_2O with the corresponding charges. At the same time, the exact distributions of these groups over the NP surfaces are not known. Furthermore, coordination states of the surface atoms on the NPs are expected to be dynamic, being dependent on the local conditions[27].

Starting from a fully atomistic model complemented with quantum mechanical *ab initio* calculations, three MD models of NP surfaces were developed with different degrees of approximations to negotiate two contrary necessities: the atomic accuracy of the NP description and the timescale of the self-assembly processes. In this respect, all these models are complementary to each other and offer different insights into the behaviour of the very complex system. Water and counterions that solvate the NPs are included explicitly at the atomistic level in all the MD simulations.

In Model 1, the description of the NP core and NP surfaces is fully atomistic with atomic charges calculated at an *ab initio* level (Fig. 4d and Supplementary Fig. 10). NPs have a 2.4 nm core with the shape of a truncated tetrahedron that closely matched the constituent NPs. The NP surfaces are coordinated by H_2O, OH^- and H^+ typical for a wide range of pH conditions. The atomic charges of a family of relevant CdS clusters in water were calculated with Gaussian software at the MP2 level, using a 6-31G basis set for H, O and S atoms, and a LanL2DZ pseudo-potential for Cd atoms. The same *ab initio* calculations were performed for the NP facets, edges and vertices. The results of both sets of calculations are consistent with each other and summarized in Supplementary Fig. 4. A net charge on the NPs can be varied with the composition of the ligand shell and was chosen to be $q = 0.3e$, $0.6e$, $0.9e$ and $1.34e$. The net NP charges match the experimental values estimated from the zeta-potential measurements for different pH conditions, namely pH 8.2, 9.2, 10.1 and 11.1.

Model 1 affords a detailed evaluation of the NP–NP processes at the interface; however, the computational cost of such a model is high. Thus, the accessible experimental timescales of the multiparticle system are short and do not allow fully equilibrated nanoshells to be reached, which necessitated the consideration of other models.

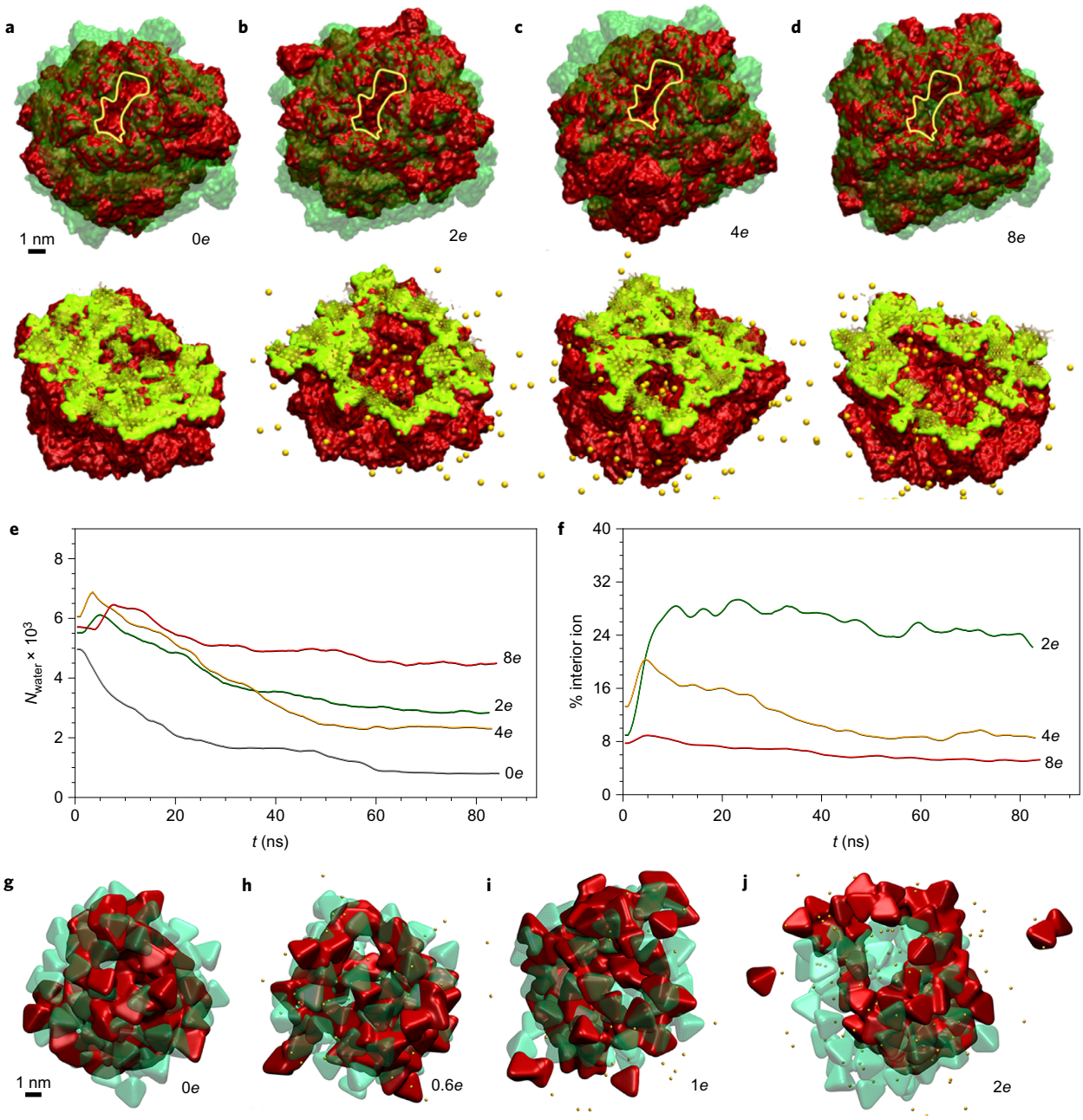

Figure 5 | Model 2 and Model 3 MD simulations of NP self-organization with progressive coarse graining and longer effective assembly times. **a**–**d**, Surface representation of the pre-assembled nanoshells taken from simulations after ~1 ns equilibration time (translucent green) and after ~85 ns equilibration time (red) for NPs in Model 2 carrying net effective charges of q = 0e (**a**), 2*e* (**b**), 4*e* (**c**) and 8*e* (**d**). The yellow lines mark the artificially formed fixed opening made to accelerate the exchange of water and ions and observe longer effective assembly times. The lower images show the corresponding cross-sections of the nanoshells. Sodium counter ions are shown by yellow spheres. Note the close similarity with TEM images in Fig. 1 and tomography data in Fig. 2. **e**,**f**, Plots of the number of water molecules (**e**) and percent of ions (**f**) inside the nanoshells in Model 2. A gradual stabilization of the number of water molecules, and thus the cavity size, is observed (Supplementary Fig. 11 gives the distribution of these ions). **g**–**j**, Surface of Model 3 nanoshells for NPs with q = 0e (**g**), 0.6e (**h**), 1e (**i**) and 2e (**j**). The translucent green shades show the initial pre-assembled nanoshells, whereas the red images show simulated structures taken from ~33 ns simulations. The nanoshells with values of Model 3 effective charge q higher than 1e destabilize due to electrostatic repulsion of NPs.

In Model 2, the NP surface carried a fixed-ratio mixture of surface ligand groups typical for high pH: $CdOH^+$, $Cd(OH)_3^-$ and $Cd(OH)_2$. Mulliken charges were obtained by *ab initio* calculations using a restricted Hartree–Fock function and a 3-21G basis set in TeraChem. The atomic charges of the O and H atoms for surface ligands were calculated *ab initio* at the MP2 level of the CHARMM force field. In the initial trials we found that Coulombic interatomic attraction between the ligands at the NP–NP interfaces results in strong bonding and sluggish reconfiguration kinetics. The collective nature and rigidity of the NP cores further contributed to the strength of these inter-NP bonds, and is essential to understand the mechanism of their formation. To access longer self-assembly times, however, the atomic charges from the ligands were placed on the NP cores to give effective charges on the NPs of q = 0*e*, 2*e*, 4*e* and 8*e*, higher than in Model 1. These values of NP charges are similar, however, to those determined experimentally for CdTe NPs carrying surface ligands of

thioglycolic acid[29]. Although having both an empirical and coarse-grained component, this approach facilitated the reconfiguration dynamics of NP structural units in the shell and allowed the simulations to address self-assembly phenomena with a large number of NPs, visualize the dynamics of the nanoshells (Supplementary Movie 2) and retain a largely atomistic description for the system.

Finally, Model 3 comprised a bare CdS core of size and geometry identical to that in Model 2 but without any surface ligands. The core-to-core vdW attraction was calculated using the Hamaker approximation typical for DLVO theory (Supplementary Methods) to accelerate the calculations. Here we also mitigated an intrinsic problem with many commonly used MD force fields. The calculations of the interatomic vdW forces are often cut off at a specific distance from the atom, typically as short as 1 nm. This approximation is acceptable for molecular systems but it is not suitable for multi-NP assemblies; the use of the DLVO-like Hamaker approximation effectively integrates the vdW interactions to infinity.

Model 1 simulations showed that the NPs become interconnected through multiple hydrogen bonds. In ~65 ns long simulations of 40 randomly dispersed NPs, the formation of small clusters, short arc-shaped chains and branched structures were observed (Fig. 4a–c) with a tendency to form more-extended assemblies with increasing $q = 0.3e$, $0.9e$ and $1.34e$. These self-assembled structures ($0.3e < q < 0.9e$) are analogous to the intermediate agglomerates that were observed during the experimental self-assembly of nanoshells (Fig. 3a–d).

Then, 81 NPs were pre-assembled into nanoshells with a radius of ~6 nm. On equilibration for ~23–29 ns, the NP reorganization led to a different and more-stable conformation of the nanoshell without any trend to fall apart. A closer view of the intermolecular contacts between the NPs reveals an extended network of hydrogen bonding between the NPs (Fig. 4e). Comparison of the TEM data in Fig. 1, tomography data in Fig. 2 and simulation data in Fig. 4 indicates that the atomistic MD models agree with the experiments.

We also monitored the total number of water molecules inside these nanoshells. This increased slightly and stabilized for $q = 0.3e$ and $0.6e$, but was not able to reach equilibrium for $q = 0.9e$ (Fig. 4f). The 'swelling' of the nanoshells that leads to the larger size of the cavities at a higher q agrees with experiment (see above). The influx of water inside the nanoshells also indicates that osmotic pressure, in addition to vdW, electrostatic interactions and hydrogen bonding, is one of the significant reasons for the transition from supraparticles to nanoshells.

In Model 2, compact nanoshells were preassembled from NPs with an artificial pore in the shell. The latter was made to accelerate the exchange of water and ions to study further the osmotic pressure role that could not be explored fully with Model 1 because of the limited effective time within the system clock. In a ~85 ns simulation, we observed a continuous reorganization of NPs in the pre-assembled large nanoshells with an extra amount of water (Supplementary Movie 2). Importantly, they underwent slow 'deflations' (Fig. 5a–d), unlike the data in Fig. 4f, which clearly indicates the tendency to produce terminal structures of specific size. Eventually, the diameter of the nanoshells plateaued and the net flow of water and ions into and out of the nanoshell approached zero (Fig. 5e–f) and reached a (meta)stable state. Similar to Model 1, the final nanoshell size in Model 2 grew with q, in agreement with experiments (Fig. 5e–f). Evaluation of the flux of water molecules and counter ions during the equilibration of the nanoshells (Supplementary Fig. 11c) confirmed that osmotic pressure takes part in the stabilization of the cavity between NPs.

Being a hybrid coarse-grained model with some atomistic components, Model 3 displayed even faster reconfiguration kinetics than the other models. Model 3 underlines the significance of multiple interfacial hydrogen bonds between the NPs. The NP–NP interfaces in these simulations do not have this attractive component and, thus, one can observe partial deconstruction of the nanoshell for effective charge of $2e$ that gave stable nanoshells in Model 2 (Fig. 5g–j). The model system display, however, stable shells for effective charges of 0, 0.6 and $1e$. Visualization of the dynamic behaviour of these assemblies also becomes possible in Model 3 (Supplementary Movie 3).

Conclusions

CdS NPs assemble spontaneously into dynamic self-limited nanoshells. These thermodynamically favourable structures exemplify the terminal self-organized systems from inorganic 'building blocks' that can occur in primitive prebiotic environment with liquid water. Although these nanoshells lack lock-and-key protein complexes or lipid-like biomacromolecules, their geometrical pH-induced behaviour can be paralleled with that of some viral capsids[30]. The simplicity of their formation and porous morphology open the road to further studies of the relationship between NP assemblies and early living systems[31] as well as to different biomimetic approaches to catalysis[32], cascade reactions[33], drug delivery[34], gene/RNA therapy and shell-like optical materials[10].

Atomistic MD simulations represent an important tool in deciphering the mechanisms of self-organization phenomena when mindfully combined with experiment and TEM imaging. However, limitations with the timescale accessible in such calculations necessitate further work on developing atomistic force fields for the needs of the NP community.

Methods

Preparation of nanoshells and their characterizations. Nanoshells were obtained by using 10^{-2} M $Cd(ClO_4)_2$ and 8×10^{-3} M thioacetamide solutions as reactants and 10^{-2} M NaOH solution to adjust the pH of the system. Typically, 2.5 ml thioacetamide solution was added into 45 ml deionized water, followed by the addition of NaOH to control the pH. More $Cd(ClO_4)_2$ solution (1 ml) was added into the above solution to initiate the formation and assembly of CdS NPs into nanoshells. TEM images were obtained on a JEOL 3011 high-resolution electron microscope. Zeta potential data were acquired by Zetasizer Nano ZS from Malvern Instruments. Typically, disposable polystyrene cuvettes were filled with sample solutions that can be put in the instrument's laser path. The system was equilibrated for two minutes to reach a stable temperature before each measurement, which consisted of 12 runs. A Smoluchowski approximation was used when converting electrophoretic mobility into zeta potential based on the Henry equation. No stable electrokinetic peaks for the dispersions with pH under 4.3 can be obtained because of the small particle size and instrumental limitations for dynamic light scattering.

Electron tomography studies. Electron tomography studies at room and cryogenic temperatures were carried out on a Tecnai F20 electron microscope (FEI Corporation) equipped with a Gatan 4 × 4 K CCD (charge coupled device) camera and a field emission gun that operated at 200 kV. At room temperature, a series of 2D projection images were recorded at a nominal magnification of 80,000 by tilting the specimen from −62° to 68° in increments of 2° < 30° and 1° > 30°. Images were recorded at an underfocus value around 1 μm. Colloidal gold 10 nm NPs were used as fiducial markers to aid tracking during the data collection and image alignment during the reconstruction. For cryoelectron tomography, 1.5 μl of a Au NP dispersion were applied to the carbon side of glow-discharged perforated R2/2 Quantifoil grids and quickly mixed with 4.5 μl of CdS nanoshell solution before plunge-freezing using a manual gravity plunger. Tomography tilt series were recorded at a nominal magnification of 80,000 by tilting the specimen from −61° to 61° in increments of 3° < 33° and 2° > 33°. Images were recorded at an underfocus value around 1 μm. For 3D reconstruction of the tilt projection series, we followed the protocols typically used in the field of the cryo-TEM tomography of soft matter[35] and, specifically, a simultaneous iterative reconstruction technique algorithm, implanted in the program TOMO3D, was allowed to run 50 iterations to calculate 3D density maps from the bin 2 tilt series[36]. The pixel size for tomographic reconstruction was 2.8 Å. A section of 268 × 326 × 131 pixels that encompassed the entire single nanoshell was cut from the complete data set. The pixel array was denoised with $k = 0.6$ for a total of eight iterations using the nonlinear anisotropic diffusion edge-enhancing algorithm available in IMOD according to a technique described previously[37,38]. The surface rendering was generated using the UCSF Chimera software package[39] with a threshold set to 4.6 and 2.8 sigma for the room temperature and cryo tomograms, respectively. The 'Segment Map' tool in UCSF Chimera performed a watershed segmentation of the NP domains with a smoothing step of four and step size of one voxel. A total of 17 regions of interconnected NPs was segmented from a single nanoshell section of the nanoshell in Fig. 2. The wall thickness and diameter were measured from the central tomographic slice of the 3D nanoshell raw volume in IMOD, instead of surface rendering. The pore size was measured using same method, but at the top slice.

MD simulations. Three computational models were used in MD simulations of the self-assembly process of CdS NPs represented as truncated tetrahedrons with a side of 2.4 nm, and *F*43*m* crystal lattice with a lattice constant $a = 0.582$ nm (Supplementary Fig. 1). In Model 1, the atomic charges of the NPs were assigned with reference to Mulliken charges obtained from *ab initio* calculations performed for small CdS clusters that represented NP surfaces and cores (Supplementary Fig. 10) in an implicit water environment using the Gaussian software package at the MP2 level with 6-31G basis set for H, O and S atoms, and a LanL2DZ pseudopotential for Cd atoms. In Models 2 and 3, the calculations were performed for the entire NP core in an implicit water environment using a GPU-powered Terachem software package (Supplementary Methods), at the restricted Hartree–Fock level with a 3-21G basis set.

The nanoshells solvated in water were pre-assembled from 81 NPs on a sphere with a radius of ~6 nm. Na^+ counter ions were added to the system to neutralize the NP charges. Partial charges of ions and TIP3P water molecules were assigned based on the CHARMM36 force field. The MD simulations were performed using the NAMD software package and the results were visualized with the VMD software package. The systems with periodic boundary conditions were simulated in an isothermal–isobaric (normal temperature and pressure) ensemble at $T = 300$ K, maintained by the Langevin dynamics with a damping coefficient of $\gamma_{Lang} = 0.01$ ps^{-1} and $P = 1$ bar. Long-range electrostatic interactions were evaluated using a particle mesh Ewald summation. Hydrophobic interactions and hydrogen bonding are taken into account through an atomistic description of the system. The Gilbert–Johnson–Keerthi algorithm was used to determine the number of water molecules and ions inside the nanoshell.

Received 26 May 2016; accepted 9 September 2016; published online 7 November 2016

References

1. Lidmar, J., Mirny, L. & Nelson, D. R. Virus shapes and buckling transitions in spherical shells. *Phys. Rev. E* **68,** 051910 (2003).
2. Settembre, C., Fraldi, A., Medina, D. L. & Ballabio, A. Signals from the lysosome: a control centre for cellular clearance and energy metabolism. *Nat. Rev. Mol. Cell Biol.* **14,** 283–296 (2013).
3. Johnstone, R. M., Adam, M., Hammond, J. R., Orr, L. & Turbide, C. Vesicle formation during reticulocyte maturation. Association of plasma membrane activities with released vesicles (exosomes). *J. Biol. Chem.* **262,** 9412–9420 (1987).
4. Tanaka, S. *et al.* Atomic-level models of the bacterial carboxysome shell. *Science* **319,** 1083–1086 (2008).
5. Bryant, D. A. & Frigaard, N.-U. Prokaryotic photosynthesis and phototrophy illuminated. *Trends Microbiol.* **14,** 488–496 (2006).
6. Hirsch, L. R. *et al.* Nanoshell-mediated near-infrared thermal therapy of tumors under magnetic resonance guidance. *Proc. Natl Acad. Sci. USA* **100,** 13549–13554 (2003).
7. Shan, Z. W. *et al.* Ultrahigh stress and strain in hierarchically structured hollow nanoparticles. *Nat. Mater.* **7,** 947–952 (2008).
8. Yu, J. & Yu, X. Hydrothermal synthesis and photocatalytic activity of zinc oxide hollow spheres. *Environ. Sci. Technol.* **42,** 4902–4907 (2008).
9. Caruso, F., Caruso, R. & Moehwald, H. Nanoengineering of inorganic and hybrid hollow spheres by colloidal templating. *Science* **282,** 1111–1114 (1998).
10. Yin, Y. *et al.* Formation of hollow nanocrystals through the nanoscale Kirkendall effect. *Science* **304,** 711–714 (2004).
11. Sun, Y., Mayers, B. & Xia, Y. Metal nanostructures with hollow interiors. *Adv. Mater.* **15,** 641–646 (2003).
12. Chang, Y., Teo, J. J. & Zeng, H. C. Formation of colloidal CuO nanocrystallites and their spherical aggregation and reductive transformation to hollow Cu_2O nanospheres. *Langmuir* **21,** 1074–1079 (2005).
13. Antonietti, M. & Förster, S. Vesicles and liposomes: a self-assembly principle beyond lipids. *Adv. Mater.* **15,** 1323–1333 (2003).
14. Hamm, C. E. *et al.* Architecture and material properties of diatom shells provide effective mechanical protection. *Nature* **421,** 841–843 (2003).
15. Xia, Y. *et al.* Self-assembly of self-limiting monodisperse supraparticles from polydisperse nanoparticles. *Nat. Nanotech.* **6,** 580–587 (2011).
16. Tang, Z., Kotov, N. A. & Giersig, M. Spontaneous organization of single CdTe nanoparticles into luminescent nanowires. *Science* **297,** 237–240 (2002).
17. Tang, Z., Zhang, Z., Wang, Y., Glotzer, S. C. & Kotov, N. A. Self-assembly of CdTe nanocrystals into free-floating sheets. *Science* **314,** 274–278 (2006).
18. Kotov, N. A., Meldrum, F. C., Wu, C. & Fendler, J. H. Monoparticulate layer and Langmuir–Blodgett-type multiparticulate layers of size-quantized cadmium sulfide clusters: a colloid-chemical approach to superlattice construction. *J. Phys. Chem.* **98,** 2735–2738 (1994).
19. Shenton, W., Pum, D., Sleytr, U. B. & Mann, S. Synthesis of cadmium sulphide superlattices using self-assembled bacterial S-layers. *Nature* **389,** 585–587 (1997).
20. Banfield, J. F. Aggregation-based crystal growth and microstructure development in natural iron oxyhydroxide biomineralization products. *Science* **289,** 751–754 (2000).
21. Cölfen, H. & Mann, S. Higher-order organization by mesoscale self-assembly and transformation of hybrid nanostructures. *Angew. Chem. Int. Ed.* **42,** 2350–2365 (2003).
22. Querejeta-Fernández, A. *et al.* Unknown aspects of self-assembly of PbS microscale superstructures. *ACS Nano* **6,** 3800–3812 (2012).
23. Zhao, G. *et al.* Mature HIV-1 capsid structure by cryo-electron microscopy and all-atom molecular dynamics. *Nature* **497,** 643–646 (2013).
24. Srivastava, S. *et al.* Light-controlled self-assembly of semiconductor nanoparticles into twisted ribbons. *Science* **327,** 1355–1359 (2010).
25. Piccinini, E., Pallarola, D., Battaglini, F. & Azzaroni, O. Self-limited self-assembly of nanoparticles into supraparticles: towards supramolecular colloidal materials by design. *Mol. Syst. Des. Eng.* **1,** 155–162 (2016).
26. Sinyagin, A. Y., Belov, A., Tang, Z. & Kotov, N. A. Monte Carlo computer simulation of chain formation from nanoparticles. *J. Phys. Chem. B* **110,** 7500–7507 (2006).
27. Silvera Batista, C. A., Larson, R. G. & Kotov, N. A. Nonadditivity of nanoparticle interactions. *Science* **350,** 1242477–1242477 (2015).
28. Vossmeyer, T. *et al.* A 'double-diamond superlattice' built up of $Cd_{17}S_4(SCH_2CH_2OH)_{26}$ clusters. *Science* **267,** 1476–1479 (1995).
29. Yaroslavov, A. A. *et al.* What is the effective charge of TGA-stabilized CdTe nanocolloids? *J. Am. Chem. Soc.* **127,** 7322–7323 (2005).
30. Kirnbauer, R., Booy, F., Cheng, N., Lowy, D. R. & Schiller, J. T. Papillomavirus L1 major capsid protein self-assembles into virus-like particles that are highly immunogenic. *Proc. Natl Acad. Sci. USA* **89,** 12180–12184 (1992).
31. Orgel, L. E. The origin of life—a review of facts and speculations. *Trends Biochem. Sci.* **23,** 491–495 (1998).
32. Rossbach, B. M., Leopold, K. & Weberskirch, R. Self-assembled nanoreactors as highly active catalysts in the hydrolytic kinetic resolution (HKR) of epoxides in water. *Angew. Chem. Int. Ed.* **45,** 1309–1312 (2006).
33. Peters, R. J. R. W. *et al.* Cascade reactions in multicompartmentalized polymersomes. *Angew. Chem.* **53,** 146–150 (2014).
34. Rösler, A., Vandermeulen, G. W. & Klok, H.-A. Advanced drug delivery devices via self-assembly of amphiphilic block copolymers. *Adv. Drug Deliv. Rev.* **53,** 95–108 (2001).
35. Nudelman, F., de With, G., Sommerdijk, N. A. J. M. Cryo-electron tomography: 3-dimensional imaging of soft matter. *Soft Matter* **7,** 17–24 (2011).
36. Agulleiro, J. I. & Fernandez, J. J. Fast tomographic reconstruction on multicore computers. *Bioinformatics* **27,** 582–583 (2011).
37. Kremer, J. R., Mastronarde, D. N. & McIntosh, J. R. Computer visualization of three-dimensional image data using IMOD. *J. Struct. Biol.* **116,** 71–76 (1996).
38. Frangakis, A. S. & Hegerl, R. Noise reduction in electron tomographic reconstructions using nonlinear anisotropic diffusion. *J. Struct. Biol.* **135,** 239–250 (2001).
39. Pettersen, E. F. *et al.* UCSF Chimera—a visualization system for exploratory research and analysis. *J. Comput. Chem.* **25,** 1605–1612 (2004).

Acknowledgements

N.A.K. is thankful to National Science Foundation (NSF) for grants CBET 0932823, CBET 1036672, DMR 1120923, DMR1403777, DMR1411014, CBET 1538180 and CHE1566460. The work is also partially supported by the US Department of Defense under grant award no. MURI W911NF-12-1-0407. We thank the University of Michigan's Electron Microscopy and Analysis Laboratory for its assistance with electron microscopy. M.Y. thanks the financial support from the National Natural Science Foundation of China (grant no. 21303032 and 21571041). P.K.'s work was supported by the NSF Division of Materials Research (grant no. 1309765) and by the American Chemical Society Petroleum Research Fund (grant no. 53062-ND6). This research used resources of the National Energy Research Scientific Computing Center, supported by the Office of Science of the US Department of Energy under contract no. DE-AC02-05CH11231, and the Extreme Science and Engineering Discovery Environment, supported by NSF (grant no. OCI-1053575) and by the National Institutes of Health (grant no. GM085043).

Author contributions

M.Y. performed the experiments, conceived the DLVO theory model and analysed the data. H.C. and P.K conceived the Gauss model and performed the MD simulations. G.Z. and P.Z. carried out and analysed the TEM tomography study. J.H.B. contributed the dynamic light-scattering experiments and calculations of the surface potential/charge of the NPs. N.A.K. conceived the project and designed the study. M.Y., H.C., P.K., G.Z., P.Z. and N.A.K. co-wrote the paper.

Additional information

Supplementary information is available in the online version of the paper. Reprints and permissions information is available online at www.nature.com/reprints. Correspondence and requests for materials should be addressed to P.Z., P.K. and N.A.K.

Competing financial interests

The authors declare no competing financial interests.